ACS EARTH AND SPACE CHEMISTRY

Article

Cite This: ACS Earth Space Chem. 2019, 3, 2307−2314

http://pubs.acs.org/journal/aesccq

The Old and the New: Aging of Sea Spray Aerosol and Formation of Secondary Marine Aerosol through OH Oxidation Reactions

Jonathan V. Trueblood,[†] Xiaofei Wang,[†] Victor W. Or,[†] Michael R. Alves,[†] Mitchell V. Santander,[†] Kimberly A. Prather,*[,†,‡] and Vicki H. Grassian*[,†,‡,§]

[†]Department of Chemistry and Biochemistry, University of California San Diego, La Jolla, California 92093, United States

[‡]Scripps Institution of Oceanography and Department of Nanoengineering, University of California, San Diego, La Jolla, California 92093, United States

[§]Department of Nanoengineering, University of California, San Diego, La Jolla, California 92093, United States

Supporting Information

ABSTRACT: In this study, we have investigated the effect of hydroxyl radical (OH) oxidation reactions on the formation and chemical composition of marine-derived aerosols. Marine aerosols can be classified into two categories: primary sea spray aerosol (SSA) produced upon the breaking of waves, and secondary marine aerosol (SMA) produced upon the oxidation of gas phase species. Here we simultaneously investigated the impact of heterogeneous OH oxidation reactions on chemically complex supermicron SSA as well as the formation of SMA in the submicron regime through the oxidation of volatile organic compounds (VOCs). A marine aerosol reference tank (MART) filled with water from a lab-grown phytoplankton bloom was used to produce SSA particles and VOCs representative of those found over the ocean, which were then sent through a potential aerosol mass (PAM) reactor where they were exposed to OH radicals. Online and offline methods were used to compare unreacted nascent primary SSA to the marine aerosols that resulted from sending the MART headspace, which includes any gases and existing primary SSA, through the PAM. Several single particle methods of analysis, including micro-Raman spectroscopy and atomic force microscopy−photothermal infrared (AFM-PTIR) spectroscopy, were used to investigate composition and size of substrate deposited particles. In situ composition measurements of PM1 particles were made using an aerosol mass spectrometer (AMS) to understand submicron marine aerosol chemistry. Raman spectra of SSA showed that heterogeneous OH oxidation reactions significantly lower the amount of organic matter found in supermicron SSA particles, which are dominated, in part, by nitrogen containing species (e.g., amino sugars/amino acids) during periods of high biological productivity. Furthermore, AFM and AMS analyses showed the formation of secondary marine aerosols in the submicron size regime due to oxidation of biologically produced VOCs. To our knowledge, this is the first study in which lab-produced authentic marine aerosols produced during a phytoplankton bloom have been exposed to OH radicals. The results provide important insights to how the combined effects of ocean biological activity and OH oxidation reactions both ultimately play roles in determining the chemical composition of marine aerosols (SMA and SSA) across multiple size regimes and formation mechanisms.

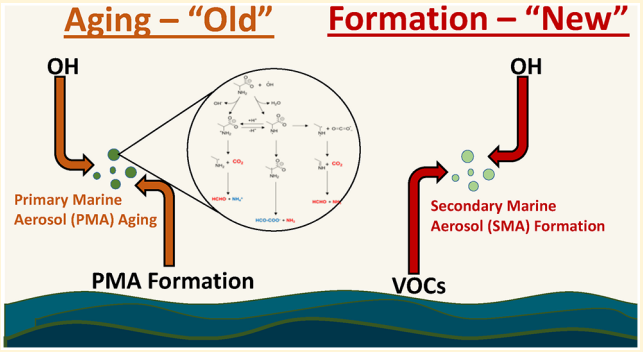

KEYWORDS: *single particle analysis, aerosol mass spectrometry, atomic force microscopy−photothermal infrared spectroscopy, phytoplankton, reaction pathways*

INTRODUCTION

Atmospheric aerosols are an important part of the Earth's system, influencing biogeochemical cycles, air quality, human health, and climate.[1] Aerosols formed in marine regions (hereafter termed marine aerosols) include primary sea spray aerosol (SSA) particles generated upon the breaking of waves, as well as secondary marine aerosol (SMA) formed upon the oxidation of volatile organic compounds (VOCs) (e.g., alkenes, dimethyl sulfide, isoprene, monoterpenes) released from the surface ocean.[2] As over two-thirds of the Earth's surface is covered by oceans, marine aerosols are an important contributor to the total global aerosol inventory.[2,3]

With respect to climate impacts, aerosols are known to alter the amount of radiation that reaches the Earth's surface both directly by scattering and absorbing solar radiation, as well as indirectly by serving as nuclei upon which water vapor and ice

Received: April 6, 2019
Revised: August 10, 2019
Accepted: August 12, 2019
Published: August 12, 2019

DOI: 10.1021/acsearthspacechem.9b00087
ACS Earth Space Chem. 2019, 3, 2307−2314

can condense to form liquid and ice droplets. A critical factor in determining the climate relevant behavior of aerosols is their physicochemical properties, which are a function of their source and formation mechanisms. Furthermore, the properties of aerosols populations can change drastically as a result of atmospheric aging processes on existing aerosols (e.g., heterogeneous photochemical reactions) and the formation of secondary aerosols by homogeneous gas-phase oxidation reactions.[4] As such, a better understanding of these processes is needed to reduce the uncertainties associated with aerosols and their impacts on climate.

It has long been known that OH radicals react with gas-phase VOCs to produce secondary organic aerosol (SOA).[5,6] However, less known is the impact of OH reactions on VOCs emitted in marine regions and the resulting secondary marine aerosols that are formed. Perhaps the most well studied VOC involved in secondary aerosol formation in marine regions is dimethylsufide (DMS). However, other VOCs such as biogenically formed isoprene and alkyl amines have also begun to receive more attention.[7] Compared to terrestrial regions, the formation of secondary aerosols in marine regions remains largely unexplained.[7]

Furthermore, recently attention has shifted to studies of the impact of OH reactions on condensed phase organic aerosols.[8] The OH-initiated oxidation of saturated hydrocarbons begins with hydrogen abstraction, followed by the formation of reactive oxygenated species (ROS). From there, functionalization reactions can lead to the formation of oxygenated low volatility species with a concomitant increase in particle mass, density, and hygroscopicity. Alternatively, fragmentation reactions via C−C bond scission can lead to the formation of higher volatility species and subsequent reduction in particle mass due to volatilization. However, attempts to determine the importance of each pathway have produced varying results: some studies have found the functionalization reactions are the dominant pathway,[9,10] while others indicate the fragmentation pathway to be of greater importance.[9,11−15] As such, the extent to which fragmentation reactions dominate varies and is difficult to predict. This is most likely dependent on chemical speciation and specific molecular species involved.

To date, studies examining the heterogeneous OH-oxidation of aerosols have focused on systems that are largely representative of terrestrial aerosols (e.g., secondary organic aerosols, particulate organic carbon aerosols, and biomass burning aerosols).[8] As previous studies have shown that the chemical composition of marine aerosol is unique from terrestrial aerosols and changes based on ocean biological activity,[16,17] marine aerosol particles are expected to exhibit different reactivities from their terrestrial counterparts. Therefore, there is a need for experiments that investigate the effects of OH-oxidation processes on authentic marine aerosol particles that account for their complex and dynamic chemical composition.

In this study, we investigate the impact of OH on the overall chemical composition of marine aerosols, through the combined effects of (1) heterogeneous OH-oxidation reactions on authentic primary supermicron SSA and (2) the formation of submicron SMA by homogeneous OH-oxidation reactions involving VOCs generated during a phytoplankton bloom. Our findings suggest that the fragmentation reactions by OH-oxidation are highly efficient for supermicron SSA particles composed of amino sugars/amino acids, which ultimately leads to losses in their particulate organic carbon mass. In addition, oxidation of VOCs was found to lead to formation of SMA, the extent of which depended on ocean biology. These results provide a better understanding of OH oxidation reactions involving biologically produced VOCs and SSA in controlling the chemical properties of the overall marine aerosol budget which includes SSA and SMA in biologically active regions of the ocean.

METHODS

Mesocosm Experiment. To replicate biological processes occurring in the ocean, an algae bloom was grown outdoors in a 2400 L tank filled with Pacific Ocean water collected from Scripps Pier (32.86 N, −117.25 W). Details of the bloom can be found in Mayer et al. (to be submitted). Phytoplankton growth was stimulated by spiking the system with an f/100 nutrient mixture (Proline, Aquatic Eco-Systems, Apopka, FL), which was diluted from the typical f/2 used in algae growth studies to generate a more realistic bloom cycle. The bloom was tracked by monitoring chlorophyll-a (chl-a) concentration, dissolved organic carbon (DOC), and bacteria counts. Chl-a concentration was determined using a Turner AquaFluor hand-held unit. Heterotrophic bacteria average concentrations and standard deviations were obtained by averaging the concentrations measured for the bulk seawater in the outdoor tank and the bulk seawater after being transferred to the MART. Enumeration was carried out by collecting samples onto 0.02 μm filters and then staining them with SYBR green dye for analysis with an epifluorescence microscope (Keyence BZ-X700).

When chl-a levels rose, 120 L of the water from the outdoor tank was transferred to a marine aerosol reference tank (MART), which then was used to generate authentic SSA. At the end of each day of the experiment, the MART was drained and refilled with water from the outdoor tank. Detailed information on the mechanism by which the MART produces SSA can be found elsewhere.[18] Briefly, the MART system uses a plunging waterfall to generate bubbles with a size distribution that reflects that of breaking waves in the ocean. Upon the bursting of surface bubbles, primary SSA were produced and then either sent directly for online and offline analyses (nascent SSA) or were sent along with the MART headspace through a potential aerosol mass (PAM) oxidative flow reactor for exposure to OH radicals before being analyzed.

Oxidation of SSA and VOCs via OH Exposure. To simulate the aging of SSA and formation of SMA through oxidation of VOCs by OH radicals, SSA and the headspace from the MART were passed through a PAM oxidative flow reactor. The PAM uses UV lamps with wavelengths of λ = 185 and 254 nm (OFR185 mode) to produce OH radicals. OH exposure was calibrated by introducing SO_2 (30 ppb) into the PAM at the same air flow rate and relative humidity used during the sampling experiments. SO_2 concentration was calculated after being passed through the PAM, and was used to calculate the OH exposure based on SO_2−OH-oxidation kinetics. The residence time of air flow in the PAM was 160 s. The OH exposure was set to be at $4.3 \pm 1.3 \times 10^{11}$ molecules·s/cm^3, which is equivalent to about 3.3 ± 0.5 days of aging under a typical atmospheric condition where OH concentrations are on the order of 1.5×10^6 molecules/cm^3.

Offline Sampling Aerosols. For offline analysis, individual nascent SSA particles exiting directly from the MART and PAM-derived aerosols (i.e., secondary marine aerosols formed through OH oxidation of VOCs and transformed, OH-aged

DOI: 10.1021/acsearthspacechem.9b00087
ACS Earth Space Chem. 2019, 3, 2307−2314

SSA) were impacted onto separate quartz and silicon wafers using stages 4 and 7 of a micro-orifice uniform deposition impactor (MOUDI, MSP Corp. Model 110), operating at a flow rate of 10 lpm for 30 min. Stage four of the MOUDI collected particles with an aerodynamic diameter between 1.8 to 3.2 μm, while stage seven sampled smaller particles between 0.32 to 0.56 μm. Samples were transferred to containers and sealed with PTFE tape inside a nitrogen purged glovebox and then stored at room temperature until analysis.

Micro-Raman Spectroscopy. Raman spectra of individual supermicron aerosol particles were collected using a LabRam HR Evolution Confocal Raman Spectrometer (Horiba). The spectrometer was equipped with an Olympus BX41 optical microscope with 100× magnification lens. Spectra were collected between 100 and 4000 cm^{-1} with a 532 nm laser. Two exposures of 10 s exposure time were averaged to obtain the resulting spectra. Each particle was then classified by comparing its spectrum to a spectral database of over 100 model systems, as done in previous studies.[17] If the Raman signal from organics in a given aerosol particle was too low, the particle was classified as sea salt (SS).

Atomic Force Microscopy−Photothermal Infrared Spectroscopy. Offline analysis via atomic force microscopy-photothermal infrared (AFM-PTIR) spectroscopy of submicron marine aerosol particles impacted on silicon wafers was conducted using a commercial nanoIR2 microscopy system (Bruker, Santa Barbara, CA, USA). AFM imaging of the particles was conducted at 298 K and a relative humidity (RH) near 30% at ambient pressure. Images were scanned at a rate of 0.5 Hz using a gold-coated silicon nitride probe (tip radius <30 nm) with 1−7 N m^{-1} spring constant and 75 ± 15 kHz resonant frequencies in tapping mode. Particle counts and their spherical volume equivalent diameter were then acquired from 20 × 20 μm^2 images (N = 9) of the particle-coated substrate. For PTIR spectroscopic analyses, AFM images were collected at a scan rate of 0.5 Hz using gold-coated silicon nitride probes (tip radius <30 nm) with 0.07−0.4 N m^{-1} spring constant and 13 ± 4 resonant frequency in contact mode. Photothermal infrared spectra were collected across the spectral range (2500−3600 cm^{-1}) with a spectral resolution of 4 cm^{-1} and by averaging 1024 laser pulses per wavenumber. Single wavenumber chemical maps were collected at a scan rate of 0.1 Hz, averaging 8 times per pixel.

Online Sampling of Aerosols. Aerosol mass was determined using a high-resolution time-of-flight aerosol mass spectrometer (HR-Tof-AMS), which characterizes non-refractory aerosol components. Briefly, dried aerosol entered the AMS through an aerodynamic focusing lens, forming a narrow particle beam which was then collected by a hot vaporizer. Nonrefractory materials were then vaporized and ionized by electron impact. Finally, a high-resolution time-of-flight mass spectrometer was used to detect the generated ions. A capture vaporizer was used in the AMS and its temperature was set to 650 °C to vaporize nonrefractory aerosol mass. AMS signals were calibrated by known mass concentration of NH_4NO_3 particles, which were produced from an atomizer. The mass size distribution was determined using AMS particle time-of-flight (PToF) mode, which separated aerosol particles based on their vacuum aerodynamic size. The detailed description of this process can be found elsewhere.[19]

RESULTS AND DISCUSSION

Biological Activity of Seawater. Figure 1 shows the changing bloom conditions over time as tracked by chl-a, DOC

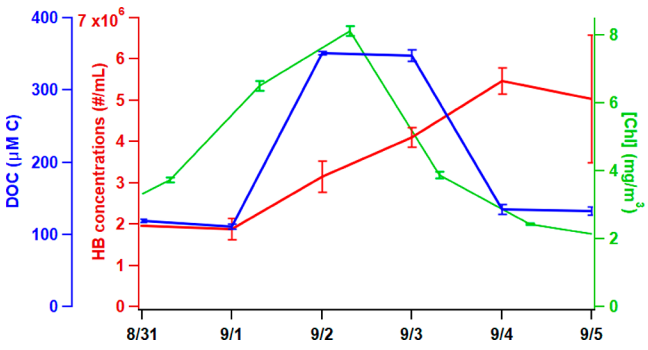

Figure 1. Seawater concentrations of dissolved organic carbon (DOC), heterotrophic bacteria (HB), and chlorophyll-a (Chl) throughout the bloom.

and bacteria concentrations. The observed conditions were similar to what is typically seen in studies using MART.[20] the start of the experiment, chl-a was at elevated levels as the bloom had already begun. Chl-a then reached a maximum on a specific date 9/2 (all experiments done in 2016) as biological activity was at a maximum, and then dropped again as the bloom died on 9/5. DOC largely correlated with chl-a concentrations, while bacteria counts lagged chl-a slightly, peaking 2 days after the chl-a maximum on 9/4.

Formation of Secondary Marine Aerosol (SMA). Figure 2 shows the AMS determined mass size distributions of organic signals for nascent SSA and PAM-derived MA (OH-exposed SSA and MART headspace). The average AMS spectra for organics in PAM-derived MA and SSA throughout the bloom

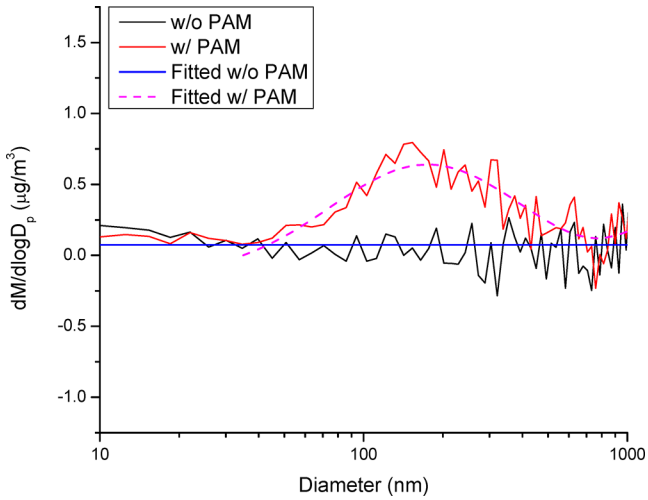

Figure 2. AMS-derived mass size distributions of organic signals and corresponding curve fits for nascent (without PAM) and PAM-derived marine aerosol. PAM-derived marine aerosol shows a significant mode which peaks at around 200 nm, which should be associated with secondary marine aerosol formation. The black curve is the average of the size-distributed organic mass spectra over 2 h without the PAM fitted to the MART system. The blue line is the fit to that signal. The red line is the size-distributed organic mass spectra over 2 h with the PAM fitted to the MART. The pink dashed line is the fit to that signal.

DOI: 10.1021/acsearthspacechem.9b00087
ACS Earth Space Chem. 2019, 3, 2307−2314

show a greater degree of oxidation for PAM-derived MA as seen by the higher fraction of mass for oxidized species (Figure S1). PAM-derived MA mass shows a significant mode that peaks at around 200 nm, which we attribute to the formation of SMA. Figure 3 shows the AMS-derived mass size

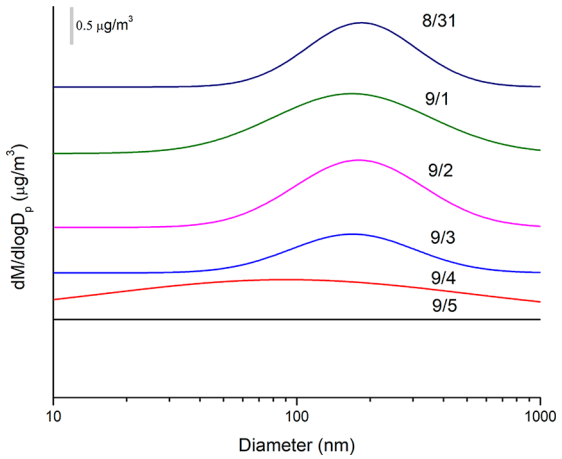

Figure 3. Curve fits of the AMS-derived mass size distributions of organic signals for PAM-derived marine aerosol on different days of the experiment. The traces are vertically offset and the scale bar denotes 0.5 $\mu g/m^3$ on the *y*-axis.

distributions of organic signals for PAM-derived MA as a function of bloom age. The SMA mode at ca. 200 nm was significant at the beginning of the bloom and decreased with bloom age toward the end of the experiment. This trend suggests that the SMA formation was associated with phytoplankton concentration in seawater. It is well-known that VOCs such as dimethyl sulfide (DMS) can form sulfate or methanesulfonic acid (MSA) secondary aerosols. Indeed, the sulfate-to-organic ratio ranged from 2 to 6 throughout the bloom. Furthermore, size distributions were also measured with a scanning mobility particle sizing (SMPS) instrument and revealed a peak maximum near 15 nm with a shoulder around 30 nm for each day. A full analysis of the sizing and AMS chemical composition data will be reported on a future manuscript, as here we are focused on the way in which OH reacts different between sub- and supermicron size regimes.

Figure 4 shows particle counts impacted on substrates as well as amplitude images (20 μm × 20 μm) of substrate deposited PAM-derived MA taken by AFM on two different days during the bloom (9/1 and 9/5). Particle counts reveal a larger number of particles in the smallest size ranges for PAM-derived MA particles at the height of the bloom (9/1) vs the end (9/5), in agreement with the data shown by AMS. Additionally, the calculated spreading ratio, defined as the maximum height of the particle divided by the maximum diameter, of PAM-derived particles at the peak of the bloom (9/1) reveals a range of values between 0.01 and 0.86, with an average of 0.272. Lower spreading ratios (i.e., <0.72 for NaCl particles) are indicative of aerosols consisting of organics that spread upon impact onto the substrate.[21] These results further point to enhanced SMA formation due to enhanced biological activity of the seawater.

AFM-PTIR spectral analysis of two submicron PAM-derived MA particles is shown in Figure 5 to further corroborate the findings by the AMS. Figure 5A shows the AFM deflection image of a particle with a volume equivalent diameter of 250

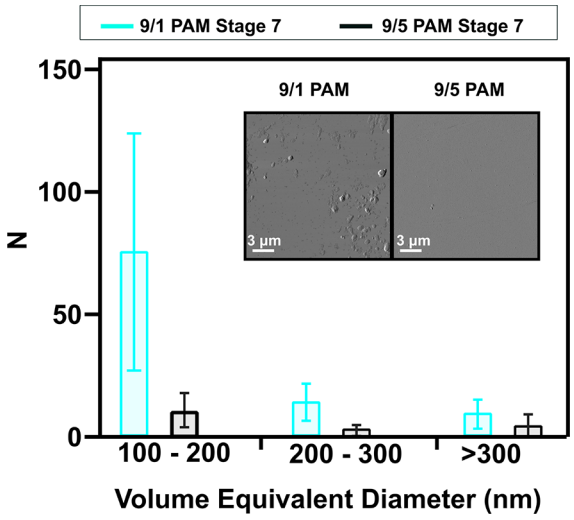

Figure 4. Average particle counts and amplitude images as measured by AFM for PAM-derived marine aerosol on 9/1 and 9/5.

nm, which according to AMS data is within the size range dominated by SMA. PTIR spectra taken at the particle shell (Figure 5B) with peaks at 2940, 2056, and 2974 ν(C−H) and 3184 ν(O−H) modes, are attributed to presence of organic species. Comparison of a 3D height image of a different particle with a volume equivalent diameter of 70 nm (Figure 5C) and its corresponding chemical map of the ν(C−H) mode at 2940 cm^{-1} (Figure 5D) also reveals the particle shell is composed largely of organics. Together, these results confirm the presence of organics in particles at both upper and lower ends of the SMA size range determined by AMS.

Fragmentation Reactions and Loss of Organic Matter in PAM-Derived MA. In addition to the formation of SMA, Raman spectroscopy of supermicron-sized PAM-derived MA particles (wet diameter = 1.8 to 3.2 μm) was conducted to investigate the impact of OH reactions on these nascent SSA particles. The particle classification and analysis method was carried out as described in previous studies.[17] The experiment combined relative contributions of each particle type for both nascent SSA and PAM-derived supermicron particles, along with their example spectra, is shown in Figure S2. The evolution of the nascent SSA particle types relative contribution (shown in Figure S3) was similar to what has been seen in other studies in which SSA was generated during a phytoplankton bloom using an ocean-atmosphere wave-flume.[17] Comparison of the Raman spectra for nascent SSA vs SSA exposed to OH revealed evidence of fragmentation reactions due to heterogeneous OH reactions with SSA, resulting in significant losses of particulate organic matter. Figure 6 shows the relative fractions of aerosols that were classified as organic, burnt/fluorescent, or sea salt according to Raman spectroscopy across all days for supermicron nascent SSA and PAM-derived MA. Additionally, as previously noted, particles were classified as sea salt if the organic signature was too low for a reasonable assignment to be made. It is important to point out that this does not mean the particle was purely sea salt, but that the contribution of organics in the particle was too low for detection with Raman spectroscopy. Particles classified as burnt/fluorescing have highly fluorescent spectra likely due to the presence of humic-like substances as well as organic components, including biological materials or have broad peaks consistent with the formation of graphitic carbon

DOI: 10.1021/acsearthspacechem.9b00087
ACS Earth Space Chem. 2019, 3, 2307−2314

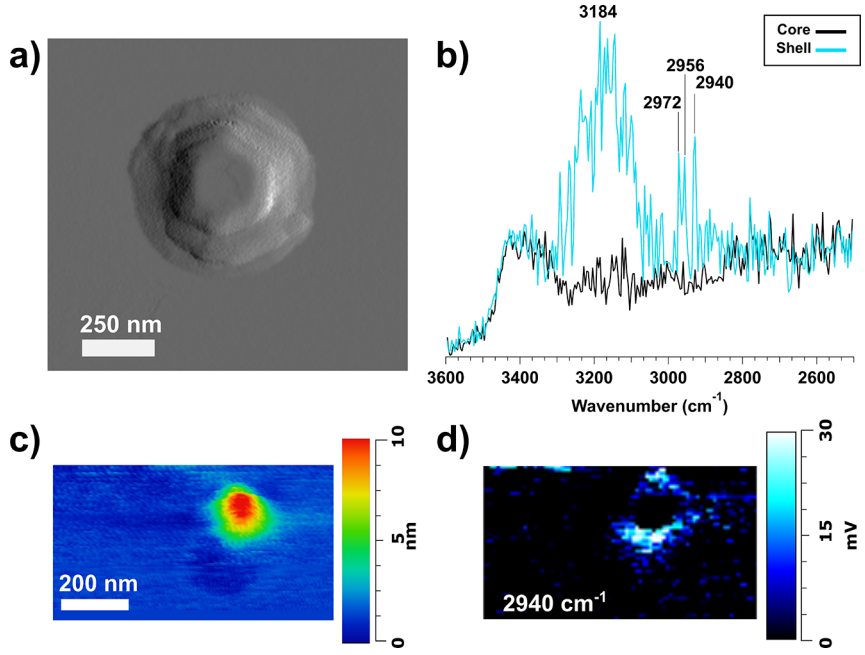

Figure 5. (a) AFM deflection image of a particle with a volume equivalent diameter of 250 nm. (b) PTIR spectra taken at the particle core (black) and on the shell (blue). (c) 3D height image of a particle with a volume equivalent diameter of 70 nm. (d) Chemical map of the particle in panel c taken at 2930 cm^{-1}.

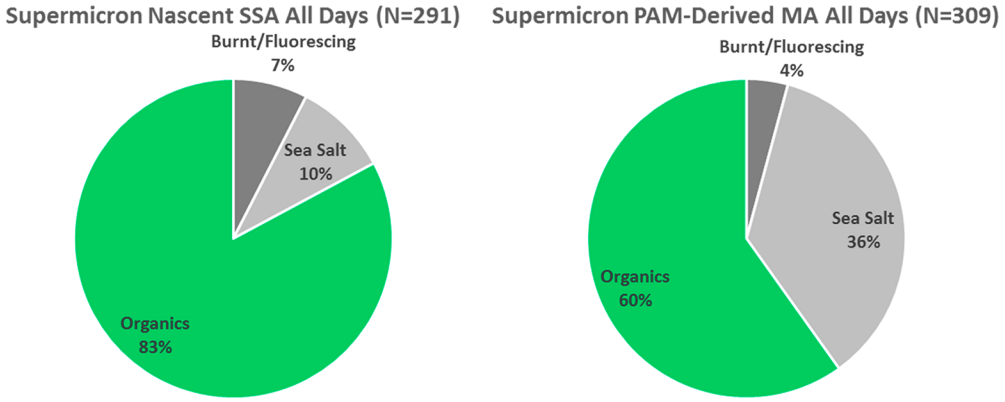

Figure 6. Relative fractions of particles that were identified as organic, burnt/fluorescing, or sea salt across all days for particles ranging from 1.8 to 3.2 μm, classified using Raman spectroscopy. Particles were classified according to a method previously described in the literature.[17] Particles that had such a small organic signature that no reasonable identification could be made were classified as sea salt particles.

due to damage from the laser beam.[22] Nascent SSA summed across all days contained 23% more organic particles than PAM-derived MA (83% vs 60%, respectively), and 26% fewer sea salt particles (10 vs 36%, respectively). The remaining 3% difference between nascent SSA and PAM-derived MA is due to a decrease in burnt/fluorescing particles from 7% to 4% between nascent SSA and PAM-derived MA, respectively.

To further explain the changes seen in supermicron particles, we examined the Raman spectra of the most common particle type in supermicron nascent SSA and PAM-derived MA particles across all days. This particle type has previously been identified as either free saccharides/amino sugars or as an alpha-amino acid such as magnesium alanine.[17,23] Figure S4 compares the spectra of this particle with that of sialic acid and alanine. Figure 7 shows the integrated area of the CH stretching region (2700 to 3100 cm^{-1}) for all nascent SSA and PAM-derived MA particles belonging to this particle type across all days. The clear drop in integrated area from nascent

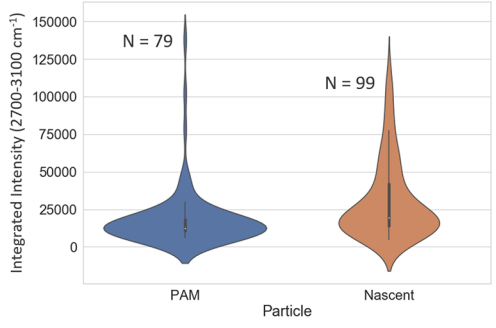

Figure 7. Violin plot of the integrated area from 2700 to 3100 cm^{-1} for of all particles classified as the most common particle type in nascent SSA and PAM-derived MA. The width of each plot represents the density distribution of particles with a given integrated area intensity.

DOI: 10.1021/acsearthspacechem.9b00087
ACS Earth Space Chem. 2019, 3, 2307−2314

SSA to PAM-derived MA suggests that the amount of organic matter present in the particles was reduced due to OH exposure. Previous studies have found that fragmentation reactions dominate in particles with O/C ratios greater than 0.4.[15] Considering alanine has an O/C ratio of 0.66, and sialic acid, a model system for amino sugars, has an O/C ratio of 0.818, it is reasonable that this particle type would be highly susceptible to fragmentation reactions due to exposure to OH radicals. Indeed, when looking at the relative contribution of each particle type for nascent SSA vs PAM-derived MA (Figures S2, S3) we see that the saccharide/amino sugar particle type had the greatest drop in relative contribution after exposure to OH radicals. The prevalence of this reactive particle type in the supermicron size regime compared to submicron particles, as identified in previous studies, further highlights the importance of the tendency for certain particle classes and organic species to be enriched in different size regimes as it may help to explain the way in which different particles undergo OH oxidation reactions.

Proposed Reaction Mechanism. A simple reaction mechanism for OH oxidation of aerosols consisting of simple hydrocarbon species has previously been proposed.[8] The first two steps of this mechanism consist of hydrogen abstraction and subsequent formation of an alkyl radical, which then reacts with O_2 to form an alkylperoxy radical (RO_2). Next, either a RO alkoxy radical is formed through self-reaction, or one of several other pathways involving reaction with HO_2, NO_x occurs. Upon formation of RO alkoxy radicals, lower-volatility oxygenated species are then either generated via isomerization reaction with O_2 and chain propagation, or lower molecular weight, higher volatility species are formed via decomposition through C−C scission.

For the chemically distinct SSA observed in our study, we propose a similar mechanism by OH radicals for an SSA particle containing amino acids such as alanine (Scheme 1). This mechanism is based on previous studies of OH initiated reactions of simple α-amino acids.[24,25] Possible products formed include CO_2, ammonia, ammonium, as well as formaldehyde (HCHO) and other radical species. Interestingly, the formation of HCHO could help to explain discrepancies seen in previous studies between HCHO observations and models.[26] However, no yields of HCHO production were measured in this study, and therefore the viability of this potential source is an important question for future studies. Again, while multiple particle classes were observed in this experiment (Figure S2), we do next expect this reaction pathway to be as important for other particle classes as it was for the most abundant particle class (i.e., free saccharides/amino sugars), as they do not contain the functional groups that are as susceptible to the proposed reaction method.

Spectroscopic evidence for this reaction mechanism is shown in the difference spectrum (PAM-derived MA − Nascent SSA) of the average of normalized Raman spectra of the most common particle type across all days (Figure 8). The effect of the loss of organics due to fragmentation and subsequent volatilization is seen in the negative peaks from 2800 to 3000 cm^{-1} which are due to symmetric and asymmetric CH stretches. Furthermore, the presence positive-going peaks indicates a greater relative contribution from ammonia, ammonium salt complexes, and NH_2-containing species as other volatile product species are lost. The positive Raman peaks between 1035 to 1070 cm^{-1}, 1550 to 1650 cm^{-1}, and 3000 to 3400 cm^{-1} are due to motions of symmetric deformation, degenerate deformation, and antisymmetric and symmetric stretching of NH_x groups present within SSA

Scheme 1. Proposed Reaction Mechanism for Loss of Organic Mass from Marine Aerosols Containing Simple Amino Sugars and Amino Acids Such as Alanine upon Exposure to OH Radicals[a]

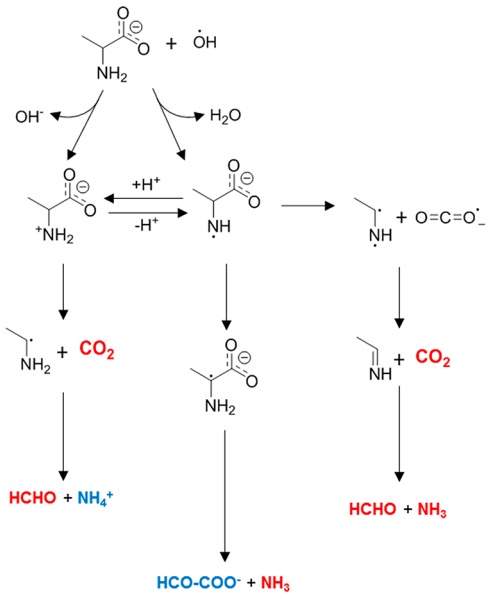

[a]Gaseous products are highlighted in red, while condensed phase products are in blue. This mechanism is based on previous studies of OH initiated reactions of simple alpha-amino acids.[22,23]

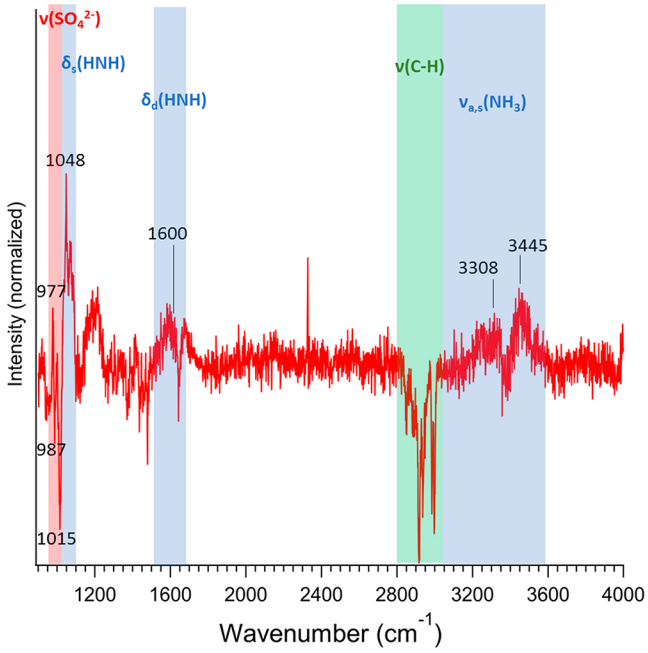

Figure 8. Difference spectrum (PAM versus non-PAM marine aerosol) of the average of the normalized Raman spectra of the most abundant particle type for supermicron SSA across all days analyzed. Inspection reveals that the SO_4^{2-} peak due to calcium sulfate decreases at 1015 cm^{-1}, while the increase in ammonium sulfate and decrease in sodium sulfate leads to a shift in the SO_4^{2-} stretch from 985 to 980 cm^{-1}.

DOI: 10.1021/acsearthspacechem.9b00087
ACS Earth Space Chem. 2019, 3, 2307−2314

including ammonium ions. These regions are highlighted in Figure 8.[27,28] Additional evidence for the formation of ammonium can be seen in the shift of the SO_4^{2-} symmetric stretching peak Figure 8. As the number of ammonium ions increase, it is expected that ammonium will interact with sulfate, leading to formation of ammonium sulfate in the aerosol. Furthermore, if enough ammonium forms, then spectral signatures due to ammonium sulfate will overwhelm the spectrum at the expense of other salt contact-ion pairs (e.g., sodium sulfate, calcium sulfate, magnesium sulfate). Indeed, what is observed is that the positive peak at lower wavenumber 977 cm^{-1} in the difference spectrum is due to SO_4^{2-} symmetric stretching of ammonium sulfate, while negative peaks at 992 and 1016 cm^{-1} are due to decrease in bands of sulfate associated with sodium and calcium ions.[29−31]

It should be noted that the efficiency of the reaction mechanism presented in Scheme 1 will depend on aerosol pH. If the aerosol is acidic, the nitrogen will remain protonated and the initial attack of the OH radical will occur on the carbon chain. Under more basic conditions, the nitrogen becomes deprotonated and competition will exist between the nitrogen and the α carbon for the initial step.[32] Above pH 6, the mechanism shown will be expected to dominate, and CO_2 yield will increase. At lower pH, this reaction may not be as important, and thus this mechanism may be most important during the early stages of aerosol lifetime as aged aerosol may have different reactivities. Additionally, recent studies have indicated that phase state can have an impact on the relevance of a given pathway.[33] Our experiments were conducted at 85% RH, meaning the particles were likely deliquesced and in aqueous phase upon exposure to OH radicals.

CONCLUSIONS

Hydroxyl radical reactions are shown to impact marine aerosol formation and composition. In particular, fragmentation reactions of supermicron particles composed of amino acids/amino sugars led to a decrease in the carbon content and formation of nitrogen-containing species (e.g., ammonium ion). AFM-PTIR analysis and AMS-derived mass analysis of submicron particles showed the formation of SMA due to oxidation of VOCs released during bloom activity. Future studies should further investigate how the dynamics of seawater microbiology could lead to subtle changes in VOC emissions, aerosol composition, and aerosol reactivity, all of which would lead to additional insights beyond what has been discussed here. Taken together, these results help to explain the complex interplay between the ocean's biological activity and atmospheric aging processes in determining the chemical composition of marine aerosols across different size-regimes.

ASSOCIATED CONTENT

Supporting Information

The Supporting Information is available free of charge on the ACS Publications website at DOI: 10.1021/acsearthspacechem.9b00087.

Figure S1 showing the average AMS spectra of PAM-derived MA and nascent SSA; Figure S2 showing the relative contribution of each supermicron particle type as determined by Raman along with their example spectra; Figure S3 showing time-resolved differences in relative particle abundance for supermicron particles; Figure S4 showing a comparison of Raman spectra for the most common particle type in supermicron particles with alanine and sialic acid model systems (PDF)

AUTHOR INFORMATION

Corresponding Authors

*E-mail: kprather@ucsd.edu.
*E-mail: vhgrassian@ucsd.edu.

ORCID

Michael R. Alves: 0000-0003-1434-5483
Vicki H. Grassian: 0000-0001-5052-0045

Notes

The authors declare no competing financial interest.

ACKNOWLEDGMENTS

The authors would like to gratefully acknowledge support by the National Science Foundation through the Centers for Chemical Innovation Program under Grant CHE1801971.

REFERENCES

(1) Poschl, U. Atmospheric Aerosols: Composition, Transformation, Climate and Health Effects. *Angew. Chem., Int. Ed.* **2005**, *44* (46), 7520−7540.

(2) Myriokefalitakis, S.; Vignati, E.; Tsigaridis, K.; Papadimas, C.; Sciare, J.; Mihalopoulos, N.; Facchini, M. C.; Rinaldi, M.; Dentener, F. J.; Cerburnis, D.; et al. Global Modeling of the Ocean Source of Organic Aerosols. *Adv. Meteorol.* **2010**, *2010*, 1−16.

(3) de Leeuw, G.; Andreas, E. L; Anguelova, M. D.; Fairall, C. W.; Lewis, E. R.; O'Dowd, C.; Schulz, M.; Schwartz, S. E. Production FLux of Sea Spray Aerosol. *Rev. Geophys.* **2011**, *80* (2010), 1−39.

(4) George, C.; Ammann, M.; D'Anna, B.; Donaldson, D. J.; Nizkorodov, S. A. Heterogeneous Photochemistry in the Atmosphere. *Chem. Rev.* **2015**, *115* (10), 4218−4258.

(5) Lim, Y. B.; Ziemann, P. J. Chemistry of Secondary Organic Aerosol Formation from OH Radical-Initaited Reactions of Linear, Branched, and Cyclic Alkanes in the Presence of NOx. *Aerosol Sci. Technol.* **2009**, *43* (6), 604−619.

(6) Lim, Y. B.; Ziemann, P. J. Products and Mechanism of Secondary Organic Aerosol Formation from Reactions of N-Alkanes with OH Radicals in the Presence of NOx. *Environ. Sci. Technol.* **2005**, *39* (23), 9229−9236.

(7) Rinaldi, M.; Decesari, S.; Finessi, E.; Giulianelli, L.; Carbone, C.; Fuzzi, S.; O'Dowd, C. D.; Ceburnis, D.; Facchini, M. C. Primary and Secondary Organic Marine Aerosol and Oceanic Biological Activity: Recent Results and New Perspectives for Future Studies. *Adv. Meterol.* **2010**, *2010*, 10.

(8) George, I. J.; Abbatt, J. P. D. Heterogeneous Oxidation of Atmospheric Aerosol Particles by Gas-Phase Radicals. *Nat. Chem.* **2010**, *2* (9), 713−722.

(9) Kessler, S. H.; Nah, T.; Daumit, K. E.; Smith, J. D.; Leone, S. R.; Kolb, C. E.; Worsnop, D. R.; Wilson, K. R.; Kroll, J. H. OH-Initiated Heterogeneous Aging of Highly Oxidized Organic Aerosol. *J. Phys. Chem. A* **2012**, *116* (24), 6358−6365.

(10) George, I. J.; Vlasenko, A.; Slowik, J. G.; Broekhuizen, K.; Abbatt, J. P. D. Heterogeneous Oxidation of Saturated Organic Aerosols by Hydroxyl Radicals: Uptake Kinetics, Condensed-Phase Products, and Particle Size Change. *Atmos. Chem. Phys.* **2007**, *7* (16), 4187−4201.

(11) Molina, M. J.; Ivanov, A. V.; Trakhtenberg, S.; Molina, L. T. Atmospheric Evolution of Organic Aerosol. *Geophys. Res. Lett.* **2004**, *31* (22), 1−5.

(12) Kroll, J. H.; Donahue, N. M.; Jimenez, J. L.; Kessler, S. H.; Canagaratna, M. R.; Wilson, K. R.; Altieri, K. E.; Mazzoleni, L. R.; Wozniak, A. S.; Bluhm, H.; et al. Carbon Oxidation State as a Metric for Describing the Chemistry of Atmospheric Organic Aerosol. *Nat. Chem.* **2011**, *3* (2), 133−139.

DOI: 10.1021/acsearthspacechem.9b00087
ACS Earth Space Chem. 2019, 3, 2307−2314

(13) Kessler, S. H.; Smith, J. D.; Che, D. L.; Worsnop, D. R.; Wilson, K. R.; Kroll, J. H. Chemical Sinks of Organic Aerosol: Kinetics and Products of the Heterogeneous Oxidation of Erythritol and Levoglucosan. *Environ. Sci. Technol.* **2010**, *44* (18), 7005−7010.
(14) Lim, C. Y.; Browne, E. C.; Sugrue, R. A.; Kroll, J. H. Rapid Heterogeneous Oxidation of Organic Coatings on Submicron Aerosols. *Geophys. Res. Lett.* **2017**, *44* (6), 2949−2957.
(15) Kroll, J. H.; Smith, J. D.; Che, D. L.; Kessler, S. H.; Worsnop, D. R.; Wilson, K. R. Measurement of Fragmentation and Functionalization Pathways in the Heterogeneous Oxidation of Oxidized Organic Aerosol. *Phys. Chem. Chem. Phys.* **2009**, *11*, 8005−8014.
(16) Wang, X.; Sultana, C. M.; Trueblood, J. V.; Hill, T. C. J.; Malfatti, F.; Lee, C.; Laskina, O.; Moore, K. A.; Beall, C. M.; McCluskey, C. S.; et al. Microbial Control of Sea Spray Aerosol Composition: A Tale of Two Blooms. *ACS Cent. Sci.* **2015**, *1* (3), 124−131.
(17) Cochran, R. E.; Laskina, O.; Trueblood, J. V.; Estillore, A. D.; Morris, H. S.; Jayarathne, T.; Sultana, C. M.; Lee, C.; Lin, P.; Laskin, J.; et al. Molecular Diversity of Sea Spray Aerosol Particles: Impact of Ocean Biology on Particle Composition and Hygroscopicity. *Chem* **2017**, *2* (5), 655−667.
(18) Stokes, M. D.; Deane, G. B.; Prather, K.; Bertram, T. H.; Ruppel, M. J.; Ryder, O. S.; Brady, J. M.; Zhao, D. A marine Aerosol Reference Tank System as a Breaking Wave ANalogue for the Production of FOam and Sea-Spray Aerosols. *Atmos. Meas. Tech.* **2013**, *6* (4), 1085−1094.
(19) Decarlo, P. F.; Kimmel, J. R.; Trimborn, A.; Northway, M. J.; Jayne, J. T.; Aiken, A. C.; Gonin, M.; Fuhrer, K.; Horvath, T.; Docherty, K. S.; et al. Field-Deployable, High-Resolution, Time-of-Flight Aerosol Mass Spectrometer. *Anal. Chem.* **2006**, *78* (24), 8281−8289.
(20) Lee, C.; Sultana, C. M.; Collins, D. B.; Santander, M. V.; Axson, J. L.; Malfatti, F.; Cornwell, G. C.; Grandquist, J. R.; Deane, G. B.; Stokes, M. D.; Azam, F.; Grassian, V. H.; Prather, K. A. Advancing Model Systems for Fundamental Laboratory Studies of Sea Spray Aerosol Using the Microbial Loop. *J. Phys. Chem. A* **2015**, *119* (33), 8860−8870.
(21) Ray, K. K.; Lee, H. D.; Gutierrez, M. A.; Chang, F. J.; Tivanski, A. V. Correlating 3D Morphology, Phase State, and Viscoelastic Properties of Individual Substrate-Deposited Particles. *Anal. Chem.* **2019**, *91*, 7621−7630.
(22) Ivleva, N. P.; McKeon, U.; Niessner, R.; Poschl, U. Raman Microspectroscopic Analysis of Size-Resolved Atmospheric Aerosol Particle Samples Collected with an ELPI: Soot, Humic-like Substances, and Inorganic Compounds. *Aerosol Sci. Technol.* **2007**, *41* (7), 655−671.
(23) Eom, H. J.; Gupta, D.; Cho, H. R.; Hwang, H. J.; Hur, S. D.; Gim, Y.; Ro, C. U. Single-Particle Investigation of Summertime and Wintertime Antarctic Sea Spray Aerosols Using Low-Z Particle EPMA, Raman Microspectrometry, and ATR-FTIR Imaging Techniques. *Atmos. Chem. Phys.* **2016**, *16* (21), 13823−13836.
(24) Vel Leitner, N. K.; Berger, P.; Legube, B. Oxidation of Amino Groups by Hydroxyl Radicals in Relation to the Oxidation Degree of the alpha-Carbon. *Environ. Sci. Technol.* **2002**, *36* (14), 3083−3089.
(25) Bonifacic, M.; Stefanic, I.; Hug, G. L.; Armstrong, D. A.; Asmus, K. D. Glycine Decarboxylation: The Free Radical Mechanism. *J. Am. Chem. Soc.* **1998**, *120* (38), 9930−9940.
(26) Riedel, K.; Allan, W.; Weller, R.; Schrems, O. Discrepancies Between Formaldehyde Measurements and Methan Oxidation Model Predictions in the Antarctic Troposphere: An Assessment of Other Possible Formaldehyde Sources. *J. Geophys. Res. D Atmos.* **2005**, *110* (15), 1−14.
(27) Ujike, T.; Tominaga, Y. Raman Spectral Analysis of Liquid AMmonia and Aqueous Solution of Ammonia. *J. Raman Spectrosc.* **2002**, *33* (6), 485−493.
(28) Sexton, B. A.; Mitchell, G. E. Vibrational Spectra of Ammonia Chemisorbed on Platinum (111) I. Identification of Chemisorbed States. *Surf. Sci.* **1980**, *99*, 523−538.
(29) Jordanov, N.; Zellner, R. Investigations of the Hygroscopic Properties of Ammonium Sulfate and Mixed AMmonium Sulfate and Glutaric Acid Micro Droplets by Means of Optical Levitation and Raman Spectroscopy. *Phys. Chem. Chem. Phys.* **2006**, *8* (23), 2759−2764.
(30) Ben Mabrouk, K.; Kauffmann, T. H.; Aroui, H.; Fontana, M. D. Raman Study of Cation Effect on Sulfate Vibrational Modes in Solid State and in Aqueous Solutions. *J. Raman Spectrosc.* **2013**, *44* (11), 1603−1608.
(31) Ault, A. P.; Zhao, D.; Ebben, C. J.; Tauber, M. J.; Geiger, F. M.; Prather, K. A.; Grassian, V. H. Raman Microspectroscopy and Vibrational Sum Frequency Generation Spectroscopy as Probes of the Bulk and Surface Compositions of Size-Resolved Sea Spray Aerosol Particles. *Phys. Chem. Chem. Phys.* **2013**, *15* (17), 6206−6214.
(32) Hayon, E.; Ibata, T.; Lichtin, N. N.; Simic, M. Sites of Attack of Hydroxyl Radicals on Amides in Aqueous Solution. *J. Am. Chem. Soc.* **1970**, *92* (13), 3898−3903.
(33) Slade, J. H.; Shiraiwa, M.; Arangio, A.; Su, H.; Poschl, U.; Wang, J.; Knopf, D. A. Cloud Droplet Activation Through Oxidation of Organic Aerosol Influenced by Temperature and Particle Phase State. *Geophys. Res. Lett.* **2017**, *44*, 1583−1591.

DOI: 10.1021/acsearthspacechem.9b00087
ACS Earth Space Chem. 2019, 3, 2307−2314